ELEMENTA
Science of the Anthropocene

Constraints from observations and modeling on atmosphere–surface exchange of mercury in eastern North America

Shaojie Song[1*] • Noelle E. Selin[1,2] • Lynne E. Gratz[3] • Jesse L. Ambrose[4] • Daniel A. Jaffe[5,6] • Viral Shah[6] • Lyatt Jaeglé[6] • Amanda Giang[2] • Bin Yuan[7,8] • Lisa Kaser[9] • Eric C. Apel[9] • Rebecca S. Hornbrook[9] • Nicola J. Blake[10] • Andrew J. Weinheimer[9] • Roy L. Mauldin III[11,12] • Christopher A. Cantrell[11] • Mark S. Castro[13] • Gary Conley[14] • Thomas M. Holsen[15] • Winston T. Luke[16] • Robert Talbot[17]

[1]Department of Earth, Atmospheric and Planetary Sciences, Massachusetts Institute of Technology, Cambridge, Massachusetts, United States
[2]Institute for Data, Systems and Society, Massachusetts Institute of Technology, Cambridge, Massachusetts, United States
[3]Environmental Program, Colorado College, Colorado Springs, Colorado, United States
[4]College of Engineering and Physical Sciences, University of New Hampshire, Durham, New Hampshire, United States
[5]School of Science, Technology, Engineering and Mathematics, University of Washington, Bothell, Washington, United States
[6]Department of Atmospheric Sciences, University of Washington, Seattle, Washington, United States
[7]Chemical Sciences Division, Earth System Research Laboratory, National Oceanic and Atmospheric Administration, Boulder, Colorado, United States
[8]Cooperative Institute for Research in Environmental Sciences, University of Colorado, Boulder, Colorado, United States
[9]Atmospheric Chemistry Observations & Modeling Laboratory, National Center for Atmospheric Research, Boulder, Colorado, United States
[10]Department of Chemistry, University of California, Irvine, Irvine, California, United States
[11]Department of Atmospheric and Oceanic Sciences, University of Colorado, Boulder, Colorado, United States
[12]Department of Physics, University of Helsinki, Helsinki, Finland
[13]Center for Environmental Science, Appalachian Laboratory, University of Maryland, Frostburg, Maryland, United States
[14]Center for Air Quality, Ohio University, Athens, Ohio, United States
[15]Department of Civil and Environmental Engineering, Clarkson University, Potsdam, New York, United States
[16]Air Resources Laboratory, National Oceanic and Atmospheric Administration, College Park, Maryland, United States
[17]Department of Earth and Atmospheric Sciences, University of Houston, Houston, Texas, United States

*song33@mit.edu

Abstract

Atmosphere–surface exchange of mercury, although a critical component of its global cycle, is currently poorly constrained. Here we use the GEOS-Chem chemical transport model to interpret atmospheric Hg^0 (gaseous elemental mercury) data collected during the 2013 summer Nitrogen, Oxidants, Mercury and Aerosol Distributions, Sources and Sinks (NOMADSS) aircraft campaign as well as ground- and ship-based observations in terms of their constraints on the atmosphere–surface exchange of Hg^0 over eastern North America. Model–observation comparison suggests that the Northwest Atlantic may be a net source of Hg^0, with high evasion fluxes in summer (our best sensitivity simulation shows an average oceanic Hg^0 flux of 3.3 ng m^{-2} h^{-1} over the Northwest Atlantic), while the terrestrial ecosystem in the summer of the eastern United States is likely a net sink of Hg^0 (our best sensitivity simulation shows an average terrestrial Hg^0 flux of -0.6 ng m^{-2} h^{-1} over the eastern United States). The inferred high Hg^0 fluxes from the Northwest Atlantic may result from high wet deposition fluxes of oxidized Hg, which are in turn related to high precipitation

Domain Editor-in-Chief
Joel D. Blum, University of Michigan

Guest Editor
Ian Michael Hedgecock, CNR Institute for Atmospheric Pollution Research

Knowledge Domains
Atmospheric Science
Earth & Environmental Science

Article Type
Research Article

Part of an *Elementa* Special Feature
Monitoring, measuring and modeling atmospheric mercury and air-surface exchange – are we making progress?

Received: November 23, 2015
Accepted: March 10, 2016
Published: April 8, 2016

rates in this region. We also find that increasing simulated terrestrial fluxes of Hg^0 in spring compared to other seasons can better reproduce observed seasonal variability of Hg^0 concentration at ground-based sites in eastern North America.

Introduction

Mercury (Hg) is a trace metal that has adverse effects on human health and the environment (Driscoll et al., 2013). Unlike most other metals, mercury in the lower atmosphere exists primarily in its elemental form (Hg^0; also known as gaseous elemental mercury, GEM), which is volatile and poorly soluble (Lin and Pehkonen, 1999). The major loss pathway of atmospheric Hg^0 is via oxidation to its oxidized state (Hg^{II}), a much more soluble form that partitions between the gas and particle phases, and subsequently undergoes dry and wet deposition (Lindberg et al., 2007; Selin, 2009). After being deposited on land and water surfaces, Hg^{II} can be reduced photochemically and/or biochemically to Hg^0, which can be reemitted back to the atmosphere (Selin et al., 2008). The atmosphere–surface exchange of Hg^0 is thus bidirectional: both evasion (upward) and dry deposition (downward) occur at the interface (Gustin and Lindberg, 2005; Xu et al., 1999). Wet deposition of Hg^0 is insignificant due to its low solubility (Maestas, 2011). A positive (negative) net flux indicates that Hg^0 evasion exceeds (is lower than) its dry deposition (Gustin et al., 2006). Hg^0 exchange fluxes are important components of global Hg emissions, which also include anthropogenic sources, geogenic activities, and biomass burning (Pirrone et al., 2010). Despite their global importance, Hg^0 fluxes from terrestrial and oceanic surfaces remain poorly constrained at global and regional scales, leading to considerable uncertainty in our understanding of the biogeochemical Hg cycle.

Based on field flux measurements and modeling studies, it remains unclear whether the global terrestrial ecosystem acts as a net source or a net sink of atmospheric Hg^0. More than 100 field studies have been conducted since the 1970s to measure terrestrial Hg^0 fluxes from various surface types (e.g., bare soil, forest, grassland, and snow/ice) and to determine environmental factors influencing Hg^0 exchange (e.g., Lindberg and Turner, 1977; Xiao et al., 1991; Poissant et al., 2004; Ferrari et al., 2005; Obrist et al., 2005; Fritsche et al., 2008; Fu et al., 2010). A recent global database summarizing these studies shows a high variability in measured Hg^0 fluxes over terrestrial surfaces (Agnan et al., 2016). Small-scale (<0.1 to 10^3 m^2) measurements, although unevenly distributed in time and among regions and landscapes, have been extrapolated to estimate terrestrial Hg^0 fluxes at a global scale (for example, (1000–3410 Mg yr^{-1}, Mason, 2009); -2810 to 4650 Mg yr^{-1} (50% uncertainty range; Agnan et al., 2016)). Agnan et al. (2016) has suggested that the largest uncertainty in estimating global terrestrial Hg^0 fluxes arises from the forest ecosystem, which has a median flux of -59 Mg yr^{-1} (a small net sink) with a very large 50% uncertainty range (-2580–3276 Mg yr^{-1}).

Most atmospheric mercury models treat Hg^0 emission from, and dry deposition to, land separately. Dry deposition is typically simulated using a resistance-in-series scheme (Wesely, 1989; Zhang et al., 2009). Some models calculate soil emissions with empirical equations involving important controlling factors such as solar radiation, temperature, and substrate Hg concentrations (Selin et al., 2008; Holmes et al., 2010; Lei et al., 2013; Lin et al., 2010; Shetty et al., 2008). Terrestrial emissions in some other models are mapped according to biogenic CO emission and/or historical Hg deposition and scaled by global Hg budgets (Dastoor et al., 2015; Chen et al., 2015; Jung et al., 2009). Simulated global Hg^0 fluxes from terrestrial surfaces range from -1300 to 3500 Mg yr^{-1} (Holmes et al., 2010; Chen et al., 2015; Lei et al., 2013; Corbitt et al., 2011; Smith-Downey et al., 2010; Kikuchi et al., 2013; Amos et al., 2013, 2014; De Simone et al., 2014). Net Hg^0 fluxes from the contiguous United States may also be positive or negative based on flux scaling methods (-183 to 269 Mg yr^{-1}, 50% uncertainty range; Agnan et al., 2016) and a newly developed bidirectional exchange model (118–141 Mg yr^{-1}, Wang et al., 2014).

The global ocean is believed to be a net Hg^0 source, but its magnitude is uncertain. Air–ocean Hg^0 exchange can be estimated using flux chamber techniques or by measuring the gradient between air Hg^0 and oceanic Hg^0 (also known as dissolved gaseous mercury, DGM) levels (Gårdfeldt et al., 2003). Most surface ocean waters have been observed to be supersaturated in DGM, generating a positive net flux of Hg^0 to the atmosphere (Sprovieri et al., 2010; Soerensen et al., 2014; Kuss et al., 2011; Ci et al., 2011a). Global Hg^0 fluxes from oceanic surfaces have been estimated in the range of 800–5500 Mg yr^{-1} by different numerical models (Strode et al., 2007; Soerensen et al., 2010; Zhang et al., 2014; De Simone et al., 2014; Lei et al., 2013; Chen et al., 2015; Amos et al., 2013, 2014; Sunderland and Mason, 2007) and using flux scaling methods (Mason and Sheu, 2002).

Atmospheric Hg^0 data can provide constraints on terrestrial and oceanic sources and sinks. For example, Hg^0 observations at a background site in Nova Scotia, Canada, show that air originating from the Northwest Atlantic has about 0.06 ng m^{-3} higher ($p < 0.05$, independent samples t-test) concentrations than air originating over terrestrial surfaces, implying Hg^0 evasion from the ocean (Cheng et al., 2014). A recent application of global-scale inverse modeling combined a global mercury model and atmospheric Hg^0 concentrations observed at multiple ground-based sites to constrain Hg^0 fluxes from terrestrial and oceanic surfaces (Song et al., 2015).

However, the relatively large systematic uncertainty (or bias) of Hg^0 concentration measurements at different sites (Slemr et al., 2015), about 10% estimated from several side-by-side intercomparison experiments (e.g., Ebinghaus et al., 1999; Temme et al., 2006), limits the assessment of terrestrial and oceanic Hg^0 fluxes across multiple sites (Song et al., 2015). This systematic uncertainty is minimized, however, when a consistent instrument is used to measure atmospheric Hg^0 at different locations. Here, we use aircraft measurements to accomplish this task. In this study, we conduct atmospheric mercury chemical transport modeling and quantitatively compare these model results with Hg^0 data from the Nitrogen, Oxidants, Mercury and Aerosol Distributions, Sources and Sinks (NOMADSS) aircraft campaign as well as ground- and ship-based observations. Our goal is to provide constraints on the large scale terrestrial and oceanic fluxes of Hg^0 from eastern North America.

Methods

In this section, we first present the aircraft-, ground-, and ship-based observations used for this study. A brief description of the GEOS-Chem Hg chemical transport model (CTM) is then given and different model simulations we perform are introduced.

Observations

Aircraft-based observations from NOMADSS

The NOMADSS campaign was conducted onboard the National Science Foundation (NSF)/National Center for Atmospheric Research (NCAR) C-130 aircraft from June 1 to July 15, 2013, during which 19 research flights were made out of Smyrna, Tennessee (Figure 1). NOMADSS was part of the Southeast Atmosphere Study (SAS; http://www.eol.ucar.edu/field_projects/sas), a field campaign that focused on southeastern U.S. regional air quality and climate. Mercury concentrations were measured using the onboard University of Washington's Detector for Oxidized Hg Species (DOHGS). Its design, configuration, and calibration have been described in detail by Lyman and Jaffe (2012) and Ambrose et al. (2013, 2015), and are briefly summarized here. The DOHGS was used to simultaneously and continuously measure total Hg (THg) and Hg^0 concentrations using two parallel channels, with Hg^{II} determined by their difference. The two channels sample ambient air at 1 standard liter per minute from a heated (110 °C) Teflon sample line connected to a rear-facing aircraft inlet. In the THg channel, air passes through a heated (650 °C) quartz pyrolyzer to reduce all Hg^{II} species to Hg^0. In the Hg^0 channel, a trapping sorbent, either quartz wool or a cation exchange membrane, is used to selectively remove Hg^{II} from the air. Each channel employs a Tekran® 2537B analyzer to detect Hg^0 at a time resolution of 2.5 minutes, using cold vapor atomic fluorescence spectrometry after pre-concentration on two alternating gold traps and subsequent thermal desorption. A customized Hg^0 permeation source was applied to perform the pre-, in-, and post-flight calibrations during NOMADSS. Mercury concentrations were reported in nanograms per cubic meter (ng m^{-3}) at standard temperature and pressure. The overall measurement uncertainty was calculated as the quadratic sum of the 1σ precision and calibration uncertainties, varying from 6–10% for Hg^0 among different research flights. The NOMADSS speciated Hg observations have been used to assess oxidation of Hg^0 by bromine in the subtropical Pacific free troposphere (Shah et al., 2016; Gratz et al., 2015), to quantify THg enhancement ratios for coal-fired power plants (Ambrose et al., 2015), and to evaluate the Hg outflow from the Chicago/Gary urban/industrial area (Gratz et al., in preparation).

Other NOMADSS measurements used here to help interpret mercury observations include isoprene, dimethyl sulfide (DMS), propane, SO_2, NO_x, and meteorological and state variables. Isoprene is known as a tracer for terrestrial forest emissions and DMS is a marker for marine emissions (Seinfeld and Pandis, 2006). Isoprene was measured using the Proton Transfer Reaction Mass Spectrometer (Yuan et al., 2015). Propane and DMS were measured by the Trace Organic Gas Analyzer, an online Gas Chromatograph Mass Spectrometer

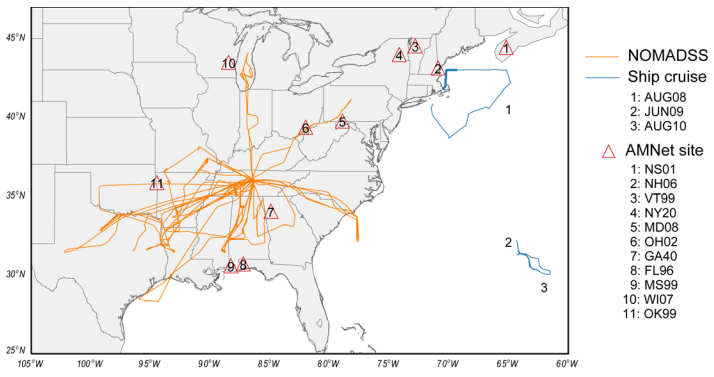

Figure 1

Aircraft-, ground-, and ship-based observations used in this study.

The orange lines are research flight tracks of the NOMADSS aircraft campaign (out of Smyrna, Tennessee, United States). The red triangles and numbers in them show the locations and names of the 11 rural/remote NADP AMNet sites. The three ship cruise routes in the Northwest Atlantic are shown in blue lines. The thick blue line for the ship cruise during August 2008 (denoted as AUG08) represents the route in the coastal Gulf of Maine where mercury observations are influenced by anomalously high freshwater input (see details in the Discussion section).

doi: 10.12952/journal.elementa.000100.f001

(Apel et al., 2010). A Thermo Scientific model 43i-TLE monitor was used to collect SO_2 data. NO_x (= NO + NO_2) data were collected from an *in situ* chemiluminescence instrument (Ridley and Grahek, 1990). We average all these measurements to a 2.5-minute resolution to be consistent with the DOHGS Hg data.

Ground- and ship-based observations

As shown in Figure 1, Hg^0 concentration observations at 11 ground-based rural/remote sites in the eastern United States are drawn from the National Atmospheric Deposition Program's Atmospheric Mercury Network (NADP AMNet). Gay et al. (2013) summarized site characteristics, as well as instrumentation, standard operating procedures, and quality assurance in the NADP AMNet network. Briefly, Tekran® analyzers are used at these sites with sampling intervals of 5–30 minutes. The original high-frequency observational data from 2009 to 2013 are converted into hourly averages and then into monthly averages. We require at least 30 minutes of data to derive an hourly average and at least 10 days of data to derive a monthly average. We use mercury observations from three summertime ship cruises (denoted AUG08, JUN09, and AUG10 for the August 2008, June 2009, and August 2010 cruises, respectively) in the Northwest Atlantic Ocean, to facilitate the analysis of net oceanic Hg^0 flux (Figure 1). Concentrations of air Hg^0, aqueous Hg^0 ($Hg_{aq}{}^0$), and total aqueous Hg ($Hg_{aq}{}^T$) along the ship cruise routes are drawn from Soerensen et al. (2013), which also described in detail the methods of atmospheric measurement and seawater collection and analysis. In addition, we compare the model outputs with the wet deposition flux of Hg^{II} in the eastern United States measured by the NADP Mercury Deposition Network (MDN) (Prestbo and Gay, 2009).

GEOS-Chem model simulations

Model description

The GEOS-Chem global CTM (version 9-02; http://www.geos-chem.org) of atmospheric composition is driven by assimilated meteorological fields from the NASA Global Modeling and Assimilation Office Goddard Earth Observing System. The GEOS-5 Forward Processing (FP) and GEOS-5.2.0 data are used for the simulation year of 2013 and the spin-up period of 2010–2012, respectively, due to their different time periods covered (http://gmao.gsfc.nasa.gov/products/). We run the CTM in a one-way nested grid formulation with the native GEOS-5 FP horizontal resolution of 0.25° × 0.3125° over North America (130–60° W, 10–60° N). The global simulation with a coarser resolution of 2° × 2.5° (degraded from the native grid) generates initial and boundary conditions for the nested grid simulation. Both simulations have 47 vertical layers in the atmosphere. The GEOS-Chem Hg nested grid simulation was developed by Zhang et al. (2012) based on GEOS-5.2.0 (with a native 0.5° × 0.667° resolution in North America), and is updated to the most recent GEOS-5 FP fields. The GEOS-Chem Hg model dynamically couples a 3D atmosphere (Selin et al., 2007), a 2D terrestrial reservoir (Selin et al., 2008), and a 2D mixed layer slab ocean (Soerensen et al., 2010). Speciated inorganic Hg tracers are tracked in both the atmosphere and the ocean mixed layer. Following Holmes et al. (2010), we include atomic bromine as the predominant oxidant of Hg^0 in the atmosphere and use a two-step oxidation mechanism (Goodsite et al., 2004, 2012). A full chemistry GEOS-Chem simulation generates tropospheric bromine fields used here (Parrella et al., 2012). Some previous Hg model simulations (e.g., Pongprueksa et al., 2011) have hypothesized photo-reduction of Hg^{II} in gas and/or aqueous phases and adjusted the reduction rates to match global mean surface Hg^0 measurements, but in our simulations, we do not include this process. Model results are sampled along flight and ship cruise routes. We use a non-local planetary boundary layer (PBL) mixing scheme developed by Holtslag and Boville (1993) and implemented in GEOS-Chem by Lin and McElroy (2010).

Atmosphere–surface exchange in the model

The surface fluxes of Hg^0 at the Earth's surface include anthropogenic sources, biomass burning, geogenic activities, as well as the bidirectional fluxes involved in the atmosphere–terrestrial and atmosphere–ocean exchange. Note that anthropogenic sources also emit a small fraction of Hg^{II}. In our model, the sink of atmospheric Hg^0 is the oxidation by bromine radicals. For all the simulations, biomass burning emissions (382 Mg yr^{-1}) are estimated using a global CO emission database (van der Werf et al., 2010) and a volume mixing ratio of Hg/CO of 2 × 10^{-7} (Slemr et al., 2014). Geogenic activities (90 Mg yr^{-1}) are spatially distributed based on the locations of mercury mines.

GEOS-Chem estimates the bidirectional exchange of Hg^0 between the atmosphere and the terrestrial and oceanic surfaces in different ways. For atmosphere–terrestrial exchange, GEOS-Chem treats the evasion and dry deposition of Hg^0 separately (Selin et al., 2008). Dry deposition is parameterized with a resistance-in-series scheme (Wesely, 1989). Hg^0 evasion includes volatilization from soil and rapid recycling of newly deposited Hg. The former is estimated as a function of soil Hg content and solar radiation. The latter is modeled by recycling a fraction of wet/dry deposited Hg^{II} to the atmosphere as Hg^0 immediately after deposition

Table 1. Global budgets of mercury from three GEOS-Chem model simulations[a]

	REF	INV	HOXSO
Hg mass in the troposphere (Mg)			
Hg^0	4230	4070	3700
Hg^{II}	520	510	550
Hg mass in the ocean mixed layer (Mg)			
Hg^0	270	250	260
Hg^{II}	3050	3950	4040
Hg emission (Mg yr^{-1})			
Hg^0, anthropogenic	1600	2290	2290
Hg^{II}, anthropogenic	340	340	340
Hg^0, net oceanic	2960	3260	3530
Hg^0, geogenic	90	90	90
Hg^0, biomass burning	380	380	380
Hg^0, soil volatilization	1700	410	610
Hg^0, quick re-evasion	580	560	600
Hg deposition (Mg yr^{-1})			
Hg^0, dry deposition over land	1320	1250	1190
Hg^{II}, dry deposition	730	700	720
Hg^{II}, wet deposition	4450	4320	4880
Hg^{II}, sea salt scavenging	1130	1070	1060
Hg redox (Mg yr^{-1})			
Oxidation of Hg^0 by BrO_x	5970	5750	6320

[a]The global budget of HOCEAN is similar to that of HOXSO, as only net oceanic Hg^0 flux from the Northwest Atlantic during summer is changed.

doi: 10.12952/journal.elementa.000100.t001

(60% for snow covered land and 20% for all other land uses) (Selin et al., 2008). The net terrestrial flux is calculated as the sum of the three individual processes. GEOS-Chem estimates the atmosphere–ocean exchange of Hg^0 using a standard two-layer diffusion model (Liss and Slater, 1974):

$$F = K(Hg_{aq}^0 - Hg_{air}^0/H) \quad (1)$$

where F is the net emission flux (ng m^{-2} h^{-1}), K is the mass transfer coefficient estimated by wind speed and temperature-corrected Schmidt numbers for CO_2 and Hg^0 (Nightingale et al., 2000), and H is a temperature dependent Henry's law constant (Andersson et al., 2008). Hg_{aq}^0 and Hg_{air}^0 are the modeled concentrations of elemental Hg in the mixed layer waters and in the lowest layer of the atmosphere, respectively. In our model, the ocean mercury in the mixed layer interacts not only with the atmospheric boundary layer but also with the subsurface waters through entrainment/detrainment of the mixed layer and wind-driven Ekman pumping (Soerensen et al., 2010).

Model simulations performed

In this study, multiple global GEOS-Chem model simulations with nested grid over North America are performed to test different representations and hypotheses of atmosphere–surface exchange of Hg^0, including a reference simulation following Song et al. (2015) referred to here as "REF", a simulation "INV" that is based on global observational constraints from inverse modeling (Song et al., 2015), and four sensitivity simulations (HSO, HOX, HOXSO, and HOCEAN). The global mercury budgets of several model simulations are shown in Table 1.

In REF, global anthropogenic mercury emissions are taken from the United Nations Environment Programme (UNEP) for 2010 (AMAP/UNEP, 2013). Over North America, UNEP 2010 emissions are replaced by U.S. EPA's National Emissions Inventory (NEI) and Environment Canada's National Pollutant Release Inventory (NPRI), both based on activity data for 2011 (U.S. EPA, 2013; Environment Canada, 2013). These inventories result in global emissions of 1598 Mg yr^{-1} Hg^0 and 340 Mg yr^{-1} Hg^{II}. Net terrestrial emission fluxes of Hg^0 can be calculated as the sum of soil volatilization, rapid recycling, and dry deposition of Hg^0 over land. In REF, the net terrestrial and oceanic fluxes of Hg^0 are 960 and 2960 Mg yr^{-1}, respectively, at a global scale (see Table 1).

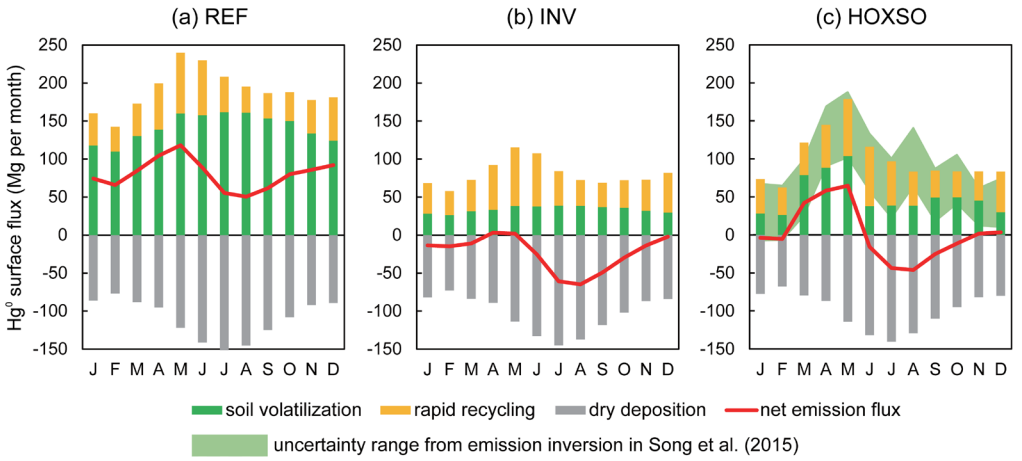

Figure 2

Seasonal variations of terrestrial fluxes of Hg^0 from three model simulations.

The monthly Hg^0 terrestrial fluxes (soil volatilization, rapid recycling, and dry deposition) modeled by REF, INV, and HOXSO are shown in (**a**), (**b**), and (**c**), respectively. The net emission flux is the sum of the three unidirectional processes. The 1σ uncertainty range from the emission inversion in Song et al. (2015) is also indicated in (**c**).

doi: 10.12952/journal.elementa.000100.f002

Song et al. (2015) optimized four model parameters and emission fluxes, including soil volatilization, Asian anthropogenic emission, and two ocean physicochemical parameters (the rate constant of dark oxidation of Hg_{aq}^{0} and the partition coefficient of Hg_{aq}^{II} on particles), using a Bayesian inversion approach and global ground-based atmospheric mercury observations. These changes are applied in the sensitivity simulation of INV. As described in detail in Song et al. (2015), the anthropogenic Asian emission of Hg^0 in the UNEP 2010 inventory is increased by 90%, and the soil volatilization in the REF is reduced by 76% (see Figure 2). Changing the two ocean parameters affects the modeled global ocean mercury budget, particularly the mass exchange between the mixed layer and subsurface waters, and also the magnitude and seasonality of Hg^0 evasion from the ocean surfaces. On a global scale, the net terrestrial and oceanic Hg^0 surface fluxes modeled by INV are -280 and 3260 Mg yr^{-1}, respectively (see Table 1).

Several sensitivity GEOS-Chem model simulations (HOX, HSO, and HOXSO; HOX standards for "high oxidation" and HSO standards for "high soil volatilization") are conducted by making additional changes to INV. The enhanced concentration levels of Hg^{II} and BrO were measured in the free troposphere during the NOMADSS aircraft campaign, supporting the role of bromine as the dominant Hg^0 oxidant (Gratz et al., 2015). Using the default tropospheric bromine fields and the oxidation mechanism (as described above), modeled Hg^{II} levels are about a factor of 3 too low (Shah et al., 2016). Therefore, in HOX, we increase the rates of Hg^0 oxidation to Hg^{II} by tripling the summertime bromine radical (BrO_x = Br + BrO) concentrations in the tropical and subtropical free troposphere (45° S–45° N; from 750 hPa to the tropopause), in order to match the observed high levels of Hg^{II} during NOMADSS. Shah et al. (2016) showed that using faster oxidation kinetics (e.g., Ariya et al., 2002) could also simulate the observed high Hg^{II} levels during NOMADSS. Recent studies have indicated that the bromine fields and kinetics used in current atmospheric models are both very uncertain (e.g., Wang et al., 2015; Ariya et al., 2015; Schmidt et al., 2015, submitted), but a detailed discussion on atmospheric oxidation and reduction is beyond the scope of this study. We hypothesize that the mid-latitude terrestrial flux of Hg^0 in spring may be enhanced based on the evidence from both atmospheric mercury modeling and surface flux measurements (see details in the Discussion section). Therefore, in HSO, the springtime soil volatilization in the mid-latitudes (20°–60°) is increased by a factor of 4 in order to evaluate this hypothesis against atmospheric observations. We will show below that this increase improves the model's ability to reproduce the seasonal pattern of observed Hg^0 concentration in the NADP AMNet network. In "HOXSO", we combine HOX and HSO by increasing both summertime oxidation and springtime soil volatilization. As shown in Table 1, these changes influence the modeled net terrestrial Hg^0 emission, Hg^0 oxidation, and Hg^{II} wet deposition. The sensitivity simulation "HOCEAN" is the same as HOXSO, except that net oceanic Hg^0 flux from the Northwest Atlantic during summer is increased by 80% (derived from the comparison between model results of HOXSO and ship cruise observations, see details in the Results section).

In the rest of the paper, these model simulation results are compared to different types of observations in eastern North America.

Results

Observed Hg^0 over terrestrial and oceanic surfaces in NOMADSS

During 19 research flights, 1589 2.5-minute observations of Hg^0 were sampled by the DOHGS. We select those observations within the planetary boundary layer (PBL), where rapid atmosphere–surface exchanges of chemical species take place. PBL heights exhibit significant spatiotemporal variations, and are typically diagnosed from vertical profiles of meteorological parameters measured by radiosonde soundings (Liu and

Liang, 2010). However, the PBL height for each NOMADSS data point cannot be determined in such a way since sounding measurements are limited in time and space (Seidel et al., 2010). Here, we select observations below the lower of 1.2 km (a fixed PBL height estimated from the vertical profile of potential temperature observed in all research flights, see Figure S1) and the modeled PBL height in the GEOS-5 FP meteorological fields. It should be noted that Kim et al. (2015) have recently shown, over the summertime southeastern United States, that the daytime GEOS-5 FP PBL heights may have a 30–50% positive bias against LIDAR and ceilometer measurements. From the sensitivity model simulations that decrease the daytime GEOS-5 FP PBL heights by 40%, we find that such potential bias does not significantly affect our simulation results and the conclusion of the paper remains unchanged. About 30% (466 data points out of 1589) of the NOMADSS Hg^0 observations are identified within the PBL. The within-PBL Hg^0 observations have a significantly larger ($p < 0.001$) median concentration of 1.47 ± 0.10 ng m^{-3} than free tropospheric Hg^0 observations (1.37 ± 0.12 ng m^{-3}), with significance determined by the non-parametric Mann-Whitney *U* test (Rosner and Grove, 1999). This vertical gradient indicates Hg^0 oxidation in the free troposphere (Shah et al., 2016). The air within the PBL is characterized by a high water vapor mixing ratio (WVMR) of 12.7 ± 1.4 g kg^{-1} whereas the free troposphere is much drier (WVMR ~ 2.2 ± 2.7 g kg^{-1}). We further remove about 3% (13 data points out of 466) of the within-PBL observations with the highest 1% of concentrations of SO_2, NO_x, or propane to avoid the influence of nearby anthropogenic sources (Ambrose et al., 2015; Miller et al., 2013). Measurements made over Lake Michigan in RF-15 are also screened out.

The selected background within-PBL NOMADSS observations are then divided into two groups: those over terrestrial and over oceanic surfaces. The air over oceanic surfaces was sampled in two flights out to the Northwest Atlantic (RF-14 and RF-16) and one flight out to the Gulf of Mexico (RF-12) (Figure 1). Measurements over terrestrial surfaces were made in 14 out of the 19 flights. The extremely low mixing ratios of isoprene (0.00 ± 0.01 ppbv) and high levels of DMS (8.26 ± 4.37 pptv) observed over oceanic surfaces, compared to those observed over terrestrial surfaces (isoprene of 1.38 ± 0.49 ppbv and DMS of 1.95 ± 1.63 pptv), suggest that the two groups represent different types of air masses (Table 2). The median Hg^0 concentration observed over oceanic surfaces (1.55 ± 0.11 ng m^{-3}, $N = 73$) is significantly higher than that over terrestrial surfaces (1.45 ± 0.09 ng m^{-3}, $N = 360$) ($p < 0.001$, Mann-Whitney *U* test).

Comparison between model and different types of observations

Below, we compare model simulation results with Hg^0 concentration observations from 11 ground-based sites, three ship cruises, and the NOMADSS campaign, as well as the wet deposition data of Hg^{II}.

Figure 3 shows the average Hg^0 concentration measured at the 11 NADP AMNet ground-based sites. The average observation in 2013 is similar to that in 2009–2012, both of which indicate pronounced seasonal variations with a maximum of Hg^0 in late winter and early spring (about 1.45 ng m^{-3} in February–April) and a minimum in late summer and early fall (about 1.20 ng m^{-3} in August–October). We use the Normalized Root Mean Square Error (NRMSE) to evaluate the performance of model simulations:

$$\mathrm{NRMSE} = \frac{\sqrt{12 \times \sum_{i=1}^{12} (Hg^0_{obs,i} - Hg^0_{mod,i})^2}}{\sum_{i=1}^{12} Hg^0_{obs,i}} \quad (2)$$

Table 2. Observed and modeled Hg^0 concentrations during NOMADSS

	Over terrestrial surfaces		Over oceanic surfaces		Mann-Whitney *U* test
	Median ± MAD	*N. of samples*	Median ± MAD	*N. of samples*	
Background within-PBL NOMADSS observations					
Hg^0 (ng m^{-3})	1.45 ± 0.09	*360*	1.55 ± 0.11	*73*	$p < 0.001$
Isoprene (ppbv)	1.38 ± 0.49	*358*	0.00 ± 0.01	*71*	$p < 0.001$
DMS (pptv)	1.95 ± 1.63	*176*	8.26 ± 4.37	*60*	$p < 0.001$
REF					
Hg^0 (ng m^{-3})	1.39 ± 0.03	*360*	1.32 ± 0.03	*73*	$p < 0.001$
INV					
Hg^0 (ng m^{-3})	1.30 ± 0.03	*360*	1.28 ± 0.02	*73*	$p = 0.45$
HOXSO					
Hg^0 (ng m^{-3})	1.29 ± 0.05	*360*	1.26 ± 0.05	*73*	$p < 0.001$
HOCEAN					
Hg^0 (ng m^{-3})	1.29 ± 0.03	*360*	1.29 ± 0.05	*73*	$p = 0.67$

doi: 10.12952/journal.elementa.000100.t002

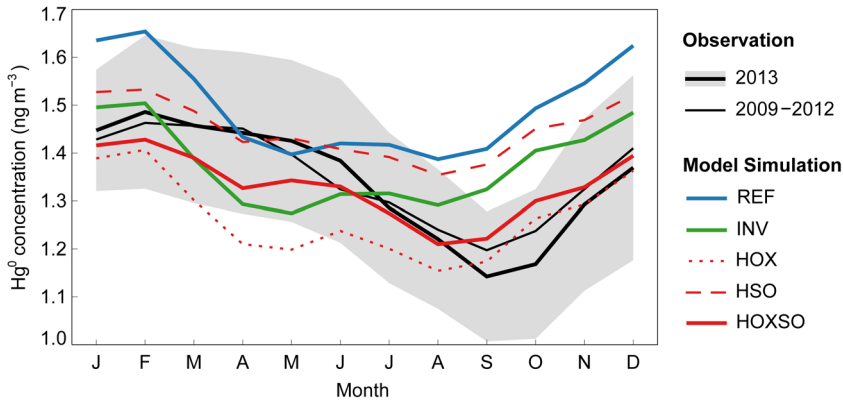

Figure 3

Averaged monthly observations and model simulations of Hg^0 concentrations for the NADP AMNet ground-based sites.

Locations of the 11 remote/rural NADP AMNet sites are plotted in **Figure 1**. The thick black line and gray shaded region show the average and 1σ uncertainty range of observed Hg^0 concentration in 2013. The thin black line shows the average observation in 2009–2012. The blue, green, and red solid lines indicate model results from REF, INV, and HOXSO, respectively. The dotted and dashed red lines indicate model results from HOX and HSO, respectively.

doi: 10.12952/journal.elementa.000100.f003

where $Hg^0_{obs,i}$ and $Hg^0_{mod,i}$ are the observed and modeled Hg^0 concentrations in the *i*th month, respectively. A smaller NRMSE value indicates a better model performance. Compared to the average NADP AMNet observation in 2013, the NRMSE values for REF, INV, HOX, HSO, and HOXSO are 0.14, 0.09, 0.09, 0.10, and 0.05, respectively, and thus HOXSO has the best performance among them. As shown in Figure 3, HOXSO is also the only simulation that reproduces the observed seasonal pattern of Hg^0 concentration. The two changes applied in HOXSO, the faster summertime Hg^0 oxidation (also made in HOX) and the elevated springtime mid-latitude soil volatilization (also made in HSO), are both essential for modeling this seasonal pattern. The tripled summertime BrO_x accelerates the conversion of Hg^0 to Hg^{II} through oxidation, and thus the modeled Hg^0 concentration in HOXSO shows a similar decreasing gradient (about -0.06 ng m^{-3} $month^{-1}$) during the summer months with the observation in 2013 (about -0.08 ng m^{-3} $month^{-1}$) and in 2009–2012 (about -0.04 ng m^{-3} $month^{-1}$). However, the model simulations without enhanced oxidation (REF, INV, and HSO) cannot reproduce this feature in the observed Hg^0 concentration. In contrast, the simulations without elevated soil volatilization (REF, INV, and HOX) show a large decline of about 0.23 ng m^{-3} in modeled Hg^0 during the spring months, which is not seen in the ground-based observations. By increasing springtime soil volatilization, HOXSO better reproduces the observed Hg^0 trend in this season. Since the two sensitivity simulations, HOX and HSO, cannot reproduce the observed seasonal pattern of ground-based Hg^0, hereafter we do not compare their results with ship cruise and aircraft measurements. Figure S2 shows the comparison of Hg^{II} wet deposition fluxes between the MDN measurements and different model simulations (REF, INV, and HOXSO) during 2013 summer over eastern North America. REF and INV have similar insignificant positive biases of +2% and +1%, respectively. This is because only Hg^0 surface fluxes differ between these two simulations. HOXSO shows a large positive bias of +59% due to the enhanced bromine radical fields used in this sensitivity simulation. It is noted that this bias should become smaller if an in-plume Hg^{II} reduction is applied in GEOS-Chem (e.g., Zhang et al., 2012).

Table 3 compares the observed and modeled concentrations of Hg in both the atmospheric boundary layer and the ocean mixed layer for three summertime ship cruises in the Northwest Atlantic Ocean (Soerensen et al., 2013). These simulations (REF, INV, and HOXSO) produce air Hg^0 concentrations (1.2–1.4 ng m^{-3}) within the uncertainty ranges of the observations. Among these simulations, REF leads to the lowest mixed layer concentrations of both Hg_{aq}^0 and Hg_{aq}^T, whereas HOXSO predicts the highest. Compared with measurements, REF and INV underestimate mixed layer Hg_{aq}^0 concentrations by 17–54% and 12–51%, respectively. HOXSO models comparable Hg_{aq}^0 concentrations for one ship cruise (AUG08), but still underestimates its levels for the other two (up to 40%). On average, HOXSO underestimates the observed mixed layer Hg_{aq}^0 by about 20%. As shown in Figure 4 (b–d), the modeled net oceanic Hg^0 emission fluxes also follow the order of REF < INV < HOXSO. Considering that HOXSO may underestimate mixed layer Hg_{aq}^0 concentrations by 40% and that different gas exchange parameterizations may lead to a 30% variability in estimated oceanic Hg^0 fluxes (Sunderland et al., 2010; Andersson et al., 2007), we conduct an additional sensitivity simulation referred to as HOCEAN, in which the net Hg^0 fluxes from the Northwest Atlantic (100–60° W, 15–45° N) during the summer months (June–July–August) are increased by 80% above the oceanic Hg^0 fluxes in HOXSO. HOCEAN thus represents a potential upper limit of oceanic emissions from the Northwest Atlantic determined from the above model–observation comparison of ship cruises.

Table 2 shows the background within-PBL Hg^0 observations during the NOMADSS aircraft campaign, divided into two groups (over terrestrial and over oceanic surfaces), and the corresponding model results from REF, INV, HOXSO, and HOCEAN. All these model simulations predict lower Hg^0 concentrations than the DOHGS observed. The modeled median concentrations of Hg^0 over terrestrial surfaces range from 1.29–1.39 ng m^{-3}, about 4–11% lower than its observed median of 1.45 ng m^{-3}. This difference generally falls within the overall measurement uncertainty range of 6–10% of the DOHGS. In contrast, by comparing the observed and modeled Hg^0 concentrations (1.33 and 1.30–1.42 ng m^{-3}, respectively) during the NOMADSS

period (2013 June–July) for the 11 AMNet ground-based sites in the eastern United States, we do not find a consistent negative bias in our model simulations (Figure 3). As described earlier, the DOHGS observed a significantly higher Hg^0 concentration of 0.10 ng m^{-3} over oceanic surfaces in the Northwest Atlantic than over terrestrial surfaces in the eastern United States. However, our model simulations cannot reproduce this land–ocean difference. As shown in Table 2, REF, INV, and HOXSO indicate that the median Hg^0 concentrations over oceanic surfaces are 0.07 ($p < 0.001$), 0.02 ($p = 0.45$), and 0.03 ($p < 0.001$) ng m^{-3} lower than those over terrestrial surfaces. HOCEAN increases the summertime net Hg^0 flux from the Northwest Atlantic by 80% than HOXSO, and predicts comparable ($p = 0.67$) Hg^0 concentrations over terrestrial surfaces (1.29 ± 0.03 ng m^{-3}) and over oceanic surfaces (1.29 ± 0.05 ng m^{-3}). Among our sensitivity GEOS-Chem model simulations, HOCEAN can be considered as the best simulation with regard to the comparison with Hg^0 observations.

Discussion

Enhanced terrestrial flux of Hg^0 in spring

We have described that HOXSO can reproduce the seasonal variation of Hg^0 concentration observed at the NADP AMNet ground-based sites with an enhanced springtime soil volatilization in the mid-latitude region (20°–60°). As shown in Figure 2, the net terrestrial fluxes of Hg^0 (the sum of soil volatilization, rapid recycling, and dry deposition) modeled by HOXSO are positive in the spring months. We hypothesize that the mid-latitude terrestrial flux of Hg^0 in spring may be enhanced based on the following evidence from both atmospheric mercury modeling and surface flux measurements. Song et al. (2015) quantitatively constrained monthly soil volatilization using worldwide ground-based observations and a Bayesian inversion approach. As shown in Figure 2, the 1σ uncertainty range of soil volatilization from the emission inversion revealed an enhancement during the spring months (Song et al., 2015), and increasing the soil volatilization by a factor of 4 agrees well with this modeling result. The measured net Hg^0 fluxes in the mid-latitudes for different land use types (i.e., forest, grassland, agriculture, and bare soil) and different seasons are summarized in Table S1. We find that most of them (7 out of 9) show higher terrestrial Hg^0 fluxes in spring (by 40% to a factor of 6) than the averages in other seasons. Bash and Miller (2007) suggested that springtime agricultural tilling operations can significantly mobilize Hg into the atmosphere from its soil pool. The small vegetation coverage in spring, which allows the penetration of solar radiation to the soil surface, may also be another important factor for the measured high Hg^0 emission fluxes (Choi and Holsen, 2009). It is important to note, however, that only limited terrestrial flux measurements are available and very large uncertainties exist in them. Net deposition fluxes of Hg^0 during springtime have also been suggested (Mao et al., 2008; Converse et al., 2010).

Implications for regional terrestrial and oceanic Hg^0 fluxes during summer

The NOMADSS aircraft campaign found higher Hg^0 concentrations over the Northwest Atlantic than over the eastern United States (Table 2). Gay et al. (2013) reported a similar finding by combining the NADP AMNet sites into several loosely defined groups, including a coastal/remote group (NS01 and NH06) and a continental/remote group (VT99, NY20, and GA40) (Figure 1). Three years of data show that the former group has about 0.07 ng m^{-3} higher Hg^0 concentrations than the latter. However, the Hg^0 measurement systematic uncertainty for these NADP AMNet sites, which is estimated to be about 0.14 ng m^{-3} (10% of the observed Hg^0 concentration of 1.3–1.4 ng m^{-3}; Figure 3), is larger than this 0.07 ng m^{-3} difference between the two site groups, limiting our ability to apply these results in a modeling context. NOMADSS minimizes potential systematic differences since the DOHGS was used to measure Hg^0 over both terrestrial and oceanic surfaces.

Table 3. Observed and modeled air and aqueous Hg for three summertime Northwest Atlantic ship cruises[a]

Hg species[b]	AUG08			JUN09			AUG10		
	air Hg^0	$Hg_{aq}^{\ 0}$	$Hg_{aq}^{\ T}$	air Hg^0	$Hg_{aq}^{\ 0}$	$Hg_{aq}^{\ T}$	air Hg^0	$Hg_{aq}^{\ 0}$	$Hg_{aq}^{\ T}$
Observation	1.4 ± 0.2	133 ± 14	1.3–2.9	1.4 ± 0.1	120 ± 7	N/R[c]	N/R[c]	196 ± 34	1.2–1.6
REF	1.40	110	1.3	1.33	78	0.9	1.31	91	1.1
INV	1.37	117	1.6	1.31	94	1.2	1.30	96	1.3
HOXSO	1.32	143	1.9	1.32	98	1.3	1.17	123	1.6

[a] Observations are obtained from Soerensen et al. (2013). For the cruise in August 2008, we exclude aqueous mercury data measured in the coastal Gulf of Maine because they were affected by anomalously high freshwater inputs.
[b] The units of air Hg^0, $Hg_{aq}^{\ 0}$, and $Hg_{aq}^{\ T}$ are ng m^{-3}, fM (10^{-12} mol m^{-3}), and pM (10^{-9} mol m^{-3}), respectively.
[c] N/R, not reported.
doi: 10.12952/journal.elementa.000100.t003

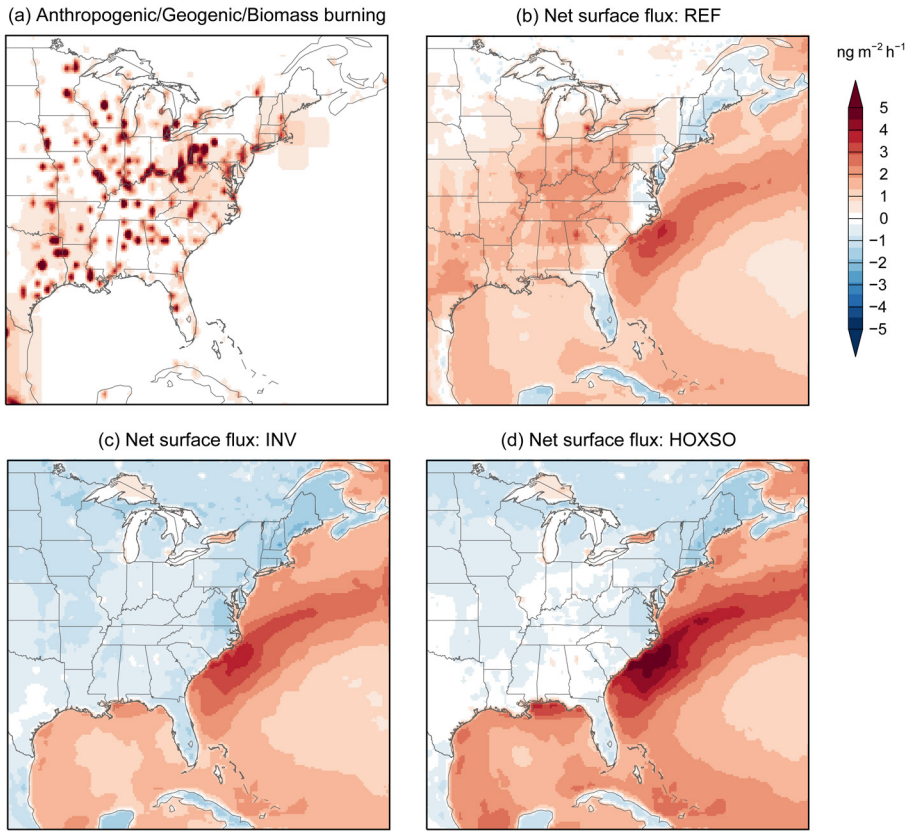

Figure 4

Spatial distributions of modeled atmospheric Hg^0 fluxes in eastern North America in summer.

The average fluxes during the summer months (June–July–August) are shown. The sum of the three unidirectional emissions (anthropogenic, geogenic, and biomass burning) is shown in (**a**). The net terrestrial and oceanic fluxes from REF, INV, and HOXSO are plotted in (**b**), (**c**), and (**d**), respectively.

doi: 10.12952/journal.elementa.000100.f004

This land–ocean difference of atmospheric Hg^0 concentrations over eastern North America has important implications for regional terrestrial and oceanic Hg^0 fluxes. The modeled net surface fluxes in 100–60° W and 20–50° N during summer are shown in Figure 4 (b–d). Note that all model simulations also include the same three unidirectional sources that occur over land (i.e., anthropogenic, geogenic, and biomass burning), which together emit 3.1 Mg month^{-1} Hg^0 from terrestrial surfaces (corresponding to an average Hg^0 flux of 0.8 ng m^{-2} h^{-1}), as shown in Figure 4a. REF emits an average net oceanic flux of 1.3 ng m^{-2} h^{-1} from the Northwest Atlantic and an average net terrestrial flux of 0.8 ng m^{-2} h^{-1} from the eastern United States. (Figure 4b). Thus, in REF, the total Hg^0 flux emitted over land (1.6 ng m^{-2} h^{-1}) is larger than that from oceanic surfaces (1.3 ng m^{-2} h^{-1}). As described earlier, in REF, the median Hg^0 over land is 0.07 ng m^{-3} higher ($p < 0.001$) than that over ocean, which is opposite to the observed land–ocean difference in NOMADSS. Among our model simulations, HOCEAN has the lowest terrestrial Hg^0 flux of -0.6 ng m^{-2} h^{-1} (total Hg^0 flux emitted over land is thus 0.2 ng m^{-2} h^{-1}) and the highest oceanic Hg^0 flux of 3.3 ng m^{-2} h^{-1}, and predicts the same Hg^0 concentrations ($p = 0.67$) over both surfaces in NOMADSS. Consequently, the above comparison between our model results and NOMADSS observations implies either even higher oceanic Hg^0 fluxes from the Northwest Atlantic or lower Hg^0 fluxes emitted from land in the eastern United States, or both, than the fluxes simulated by HOCEAN.

We have demonstrated through the model–observation comparison of ship cruises that HOCEAN represents a potential upper limit of oceanic emissions from the Northwest Atlantic. However, riverine discharges of Hg, an oceanic source that is not considered in the 2D mixed layer slab ocean of GEOS-Chem, may lead to additional Hg^0 emissions from coastal/shelf areas and help to reconcile the difference between model results and NOMADSS observations. Soerensen et al. (2013) found, during the ship cruise AUG08 in the Northwest Atlantic (Figure 1), that enhanced freshwater inputs due to anomalously high precipitation in July 2008 strongly increased the mixed layer Hg_{aq}^0 concentrations and Hg^0 fluxes in waters of the Gulf of Maine approximately 60 km offshore (270 ± 50 fM and 7.2 ± 4.2 ng m^{-2} h^{-1}), when compared to those in more open waters (130 ± 14 fM and 3.8 ± 2.9 ng m^{-2} h^{-1}). A spatial trend of higher Hg_{aq}^0 levels in coastal waters (~ 100 km) than in open waters has also been observed in other cruises (e.g., Ci et al., 2011b). Two NOMADSS research flights, RF-14 and RF-16, sampled the oceanic air 50–150 km off the coast of South Carolina on July 5 and July 8 of 2013, respectively (Figure 1). Unusually high water discharges were measured in July 2013 for rivers in South Carolina (see Figure S3a for an example). Additionally, measurements within the NADP Mercury Deposition Network (MDN; Prestbo and Gay, 2009) showed heavy rainfall and high

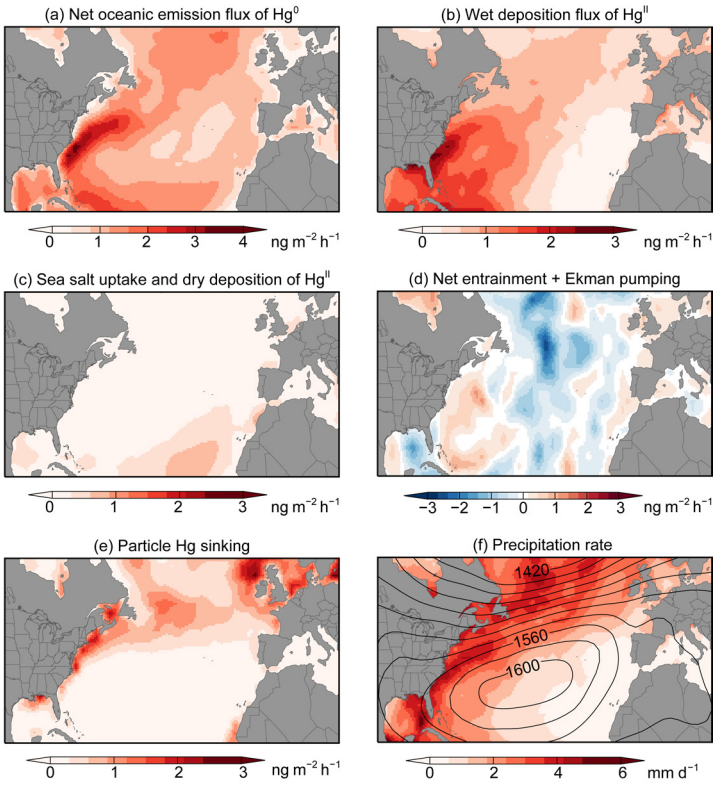

Figure 5

Spatial distributions of modeled vertical exchange fluxes in the North Atlantic in summer.

Model results from HOXSO are shown. The plots in (**a**–**e**) indicate different mercury exchange fluxes between the atmosphere and the mixed layer and between the mixed layer and subsurface waters. The spatial distribution of precipitation rate is shown in (**f**) overlaid with geopotential height contour lines at 850 hPa. The geopotential height data are obtained from the NCEP/NCAR reanalysis (http://www.esrl.noaa.gov/psd/data/gridded/reanalysis/).

doi: 10.12952/journal.elementa.000100.f005

wet deposition fluxes of Hg in late June and early July 2013, right before the sampling time of these two flights (see Figure S3b for an example). Overall, these results suggest that riverine discharges of mercury may contribute to the observed high Hg^0 concentration over the Northwest Atlantic.

HOCEAN simulates an average net terrestrial flux of -0.6 ng m^{-2} h^{-1}, meaning that the simulated terrestrial ecosystem in the eastern United States is a net sink of Hg^0 during summer. The simulated dry deposition of Hg^0 of 2.0 ng m^{-2} h^{-1} is only partially offset by its evasion that includes soil volatilization (0.6 ng m^{-2} h^{-1}) and rapid recycling of newly deposited Hg (0.8 ng m^{-2} h^{-1}). The global terrestrial flux measurement database (Agnan et al., 2016) suggests a small positive median Hg^0 flux of 0.1 ng m^{-2} h^{-1} (50% uncertainty range: -0.1 to 0.5 ng m^{-2} h^{-1}) over background bare soil, which is in agreement with measured vertical profiles of Hg^0 in soil pores (Obrist et al., 2014). However, forest is the most important land use type in the eastern United States, especially during summer when the leaf area index is maximum (thus leaf surface areas are several times larger than underlying soil surface areas) (Drummond and Loveland, 2010; Buermann et al., 2001). Forest canopies can reduce Hg^0 evasion from underlying soils by absorbing most of the incoming solar radiation and suppressing the rising of soil temperature (Wang et al., 2006; Choi and Holsen, 2009). Foliage is well-known to constitute a net sink of atmospheric Hg^0 through stomatal and non-stomatal uptake (Wang et al., 2014; Stamenkovic and Gustin, 2009), and the median Hg^0 flux measured over leaves at background forest sites is -0.12 ng m^{-2} h^{-1} with a 50% uncertainty range from -1.48 to 1.65 ng m^{-2} h^{-1} (Agnan et al., 2016). Hg translocation from soil to leaves is unlikely to be significant (Fay and Gustin, 2007; Cui et al., 2014). Therefore, it is not unreasonable to consider the summertime terrestrial ecosystem in the eastern United States as a net sink of Hg^0, given relatively low soil evasion and high foliage uptake. However, it is not possible to provide an accurate estimate for the magnitude of this sink, since reliable flux measurements over forests are currently lacking, and the mechanism of Hg transport in plant/vegetation is not well understood (Agnan et al., 2016).

The unidirectional sources over land (i.e., anthropogenic, geogenic, and biomass burning) are also uncertain and their fluxes may be higher or lower than the values applied in our model. However, their uncertainties are small compared to those associated with terrestrial and oceanic fluxes in the studied region. In summer, simulated geogenic activities and biomass burning emit little atmospheric Hg^0 from the eastern United States (< 0.1 ng m^{-2} h^{-1} on average), and thus the contributions of their uncertainties on Hg^0 fluxes are insignificant in this context. The NEI 2011 inventory used in our model has an average Hg^0 flux of 0.7 ng m^{-2} h^{-1} in the eastern United States. In general, anthropogenic emissions in North America are considered to be relatively well constrained (1σ error around ± 30%) (e.g., Pacyna et al., 2010; AMAP/UNEP, 2013). Although U.S. EPA will not release the NEI inventory in 2013 (the year in which NOMADSS took place), another estimate, the Toxics Release Inventory (TRI; U.S. EPA, 2015), shows that the magnitudes of estimated mercury emissions for 2011 and 2013 differ only slightly (< 2%).

Origin of high Hg^0 flux from the Northwest Atlantic

Based on the comparison between model results and aircraft and ship cruise observations, our analysis suggests a high Hg^0 flux from the Northwest Atlantic. In our simulations, this high Hg^0 flux helps to explain the land–ocean differences of observed atmospheric Hg^0 concentrations in the eastern North America, and also agrees with the observed high aqueous Hg^0 levels in the mixed layer. In contrast, a recent study by Weigelt et al. (2015) classified Hg^0 data observed at the Mace Head station on the Northeastern Atlantic coast of Ireland into different air mass groups according to their geographical origins. Air masses originating mostly from the Northeast Atlantic were found to have generally lower Hg^0 concentrations (0.07 ± 0.04 ng m^{-3} calculated from monthly means and 0.04 ± 0.05 ng m^{-3} from monthly medians, both using data in 2010–2013) than those from continental Europe. As shown in Figure S4, our model simulations of the Northwest Atlantic, particularly the waters near the continental United States, have overall higher Hg^0 fluxes when compared to the Northeast Atlantic. This is qualitatively consistent with the different land–ocean patterns of observed atmospheric Hg^0 over the Northeast and Northwest Atlantic.

The model also enables us to identify physicochemical processes that lead to simulated high Hg^0 fluxes in the Northwest Atlantic (and the relatively low fluxes in the Northeast Atlantic). The modeled Hg^0 fluxes are positively correlated with the mixed layer Hg_{aq}^0 concentrations (Equation 1), which are in turn determined by multiple processes in the mixed layer, including photochemical- and biological- redox reactions and adsorption/desorption on particles, and the vertical interactions of the mixed layer with the above atmosphere and subsurface waters. The wet/dry deposition of Hg^{II} from the atmosphere is a source of mercury in the mixed layer, whereas Hg^0 evasion into the atmosphere is a sink. Vertical exchanges between the mixed layer and subsurface waters include entrainment/detrainment, wind-driven Ekman pumping, and particle sinking (biological carbon pump) (Soerensen et al., 2010; Batrakova et al., 2014; Song et al., 2015). Figure 5a shows the spatial distribution of net Hg^0 fluxes (modeled by HOXSO) from the North Atlantic Ocean (100° W–20° E, 20–60° N) in summer. The spatial distributions of modeled Hg fluxes associated with several above-mentioned processes are shown in Figure 5(b–e). A comparison of the magnitude of these Hg fluxes indicates that the high wet deposition of Hg^{II} into the Northwest Atlantic is the dominant process determining the simulated high net oceanic flux of Hg^0 from this region. The wet deposition of Hg^{II} is closely related to the precipitation rate, which also has a spatial pattern with generally higher values in the Northwest Atlantic, in particular the waters near the continental United States, and lower values in the Northeast Atlantic (see Figure 5f). The summertime precipitation in the North Atlantic is influenced by the North Atlantic Subtropical High (NASH, also known as the Bermuda High), a semi-permanent high pressure system in the lower troposphere (Li et al., 2012). As shown in Figure 5f, strong precipitation is located along the western boundary of the NASH, which can be represented by the 1560 m geopotential contour line at 850 hPa (Li et al., 2011), while the precipitation rate in eastern side of the NASH is very small. Overall, the high simulated Hg^0 flux from the Northwest Atlantic is mainly a result of high wet deposition of Hg^{II}, which is in turn linked to high precipitation rates in this region during summer. Given the uncertainties in modeling oceanic mercury and the limited representation of these processes in our slab ocean model, however, our ability to draw process-based conclusions from this study is limited. Similarly, a more detailed 3D oceanic mercury model (Zhang et al., 2014) suggests that high wet deposition of Hg^{II} leads to high Hg^0 flux from the Northwest Atlantic (Zhang Y, personal communication).

Conclusions

Atmosphere–surface exchange of Hg^0 in eastern North America is constrained by combining aircraft-based observations made during the 2013 summer NOMADSS campaign (as well as ground- and ship-based measurements) and GEOS-Chem CTM simulations. As a consistent instrumentation (the DOHGS) measured Hg throughout NOMADSS, the systematic uncertainty of Hg^0 concentration measurements at different locations is minimized. Within the PBL, significantly higher median Hg^0 concentrations were observed over oceanic surfaces of the Northwest Atlantic than over terrestrial surfaces of the eastern United States during NOMADSS ($p < 0.001$). The model simulation (HOCEAN) with a low (negative) terrestrial Hg^0 flux and a high (positive) oceanic flux in this region obtains the same Hg^0 concentrations ($p = 0.67$) over both surfaces. Riverine discharges of mercury, an oceanic source that is not included in GEOS-Chem but may be significant in the NOMADSS period, may help to reconcile the model–observation discrepancy. By analyzing processes in the 2D mixed layer slab ocean of GEOS-Chem, we show that inferred high Hg^0 emission fluxes from the Northwest Atlantic may be a result of high wet deposition fluxes of oxidized mercury, which are in turn linked to high precipitation rates in this region. Given relatively low soil evasion and high foliage uptake, it is likely that terrestrial ecosystem in the summer eastern United States acts as a net sink of Hg^0. Increasing simulated terrestrial fluxes of Hg^0 in spring compared to other seasons can better reproduce seasonal variability of observed Hg^0 concentration at ground-based sites in eastern North America.

References

Agnan Y, Le Dantec T, Moore CW, Edwards GC, Obrist D. 2016. New constraints on terrestrial surface–atmosphere fluxes of gaseous elemental mercury using a global database. *Environ Sci Technol* **50**(2): 507–524. doi:10.1021/acs.est.5b04013.

AMAP/UNEP. 2013. Technical background report for the Global Mercury Assessment 2013. *Arctic Monitoring and Assessment Programme, Oslo, Norway/UNEP Chemicals Branch Geneva, Switzerland*. http://www.amap.no/documents/doc/technical-background-report-for-the-global-mercury-assessment-2013/848. Accessed February 2, 2016.

Ambrose JL, Gratz LE, Jaffe DA, Campos T, Flocke FM, et al. 2015. Mercury emission ratios from coal-fired power plants in the Southeastern United States during NOMADSS. *Environ Sci Technol* **49**(17): 10389–10397. doi: 10.1021/acs.est.5b01755.

Ambrose JL, Lyman SN, Huang J, Gustin MS, Jaffe DA. 2013. Fast time resolution oxidized mercury measurements during the Reno Atmospheric Mercury Intercomparison Experiment (RAMIX). *Environ Sci Technol* **47**(13): 7285–7294. doi: 10.1021/es303916v.

Amos HM, Jacob DJ, Kocman D, Horowitz HM, Zhang Y, et al. 2014. Global biogeochemical implications of mercury discharges from rivers and sediment burial. *Environ Sci Technol* **48**(16): 9514–9522. doi: 10.1021/es502134t.

Amos HM, Jacob DJ, Streets DG, Sunderland EM. 2013. Legacy impacts of all-time anthropogenic emissions on the global mercury cycle. *Global Biogeochem Cy* **27**(2): 410–421. doi: 10.1002/gbc.20040.

Andersson ME, Gårdfeldt K, Wängberg I, Sprovieri F, Pirrone N, et al. 2007. Seasonal and daily variation of mercury evasion at coastal and off shore sites from the Mediterranean Sea. *Mar Chem* **104**(3–4): 214–226. doi:10.1016/j.marchem.2006.11.003.

Andersson ME, Gårdfeldt K, Wängberg I, Strömberg D. 2008. Determination of Henry's law constant for elemental mercury. *Chemosphere* **73**(4): 587–592. doi: 10.1016/j.chemosphere.2008.05.067.

Apel EC, Emmons LK, Karl T, Flocke F, Hills AJ, et al. 2010. Chemical evolution of volatile organic compounds in the outflow of the Mexico City Metropolitan area. *Atmos Chem Phys* **10**(5): 2353–2375. doi: 10.5194/acp-10-2353-2010.

Ariya PA, Amyot M, Dastoor A, Deeds D, Feinberg A, et al. 2015. Mercury physicochemical and biogeochemical transformation in the atmosphere and at atmospheric interfaces: A review and future directions. *Chem Rev* **115**(10): 3760–3802. doi: 10.1021/cr500667e.

Ariya PA, Khalizov A, Gidas A. 2002. Reactions of gaseous mercury with atomic and molecular halogens: Kinetics, product studies, and atmospheric implications. *J Phys Chem A* **106**(32): 7310–7320. doi: 10.1021/jp020719o.

Bash JO, Miller DR. 2007. A note on elevated total gaseous mercury concentrations downwind from an agriculture field during tilling. *Sci Total Environ* **388**(1–3): 379–388. doi: 10.1016/j.scitotenv.2007.07.012.

Batrakova N, Travnikov O, Rozovskaya O. 2014. Chemical and physical transformations of mercury in the ocean: A review. *Ocean Sci* **10**(6): 1047–1063. doi: 10.5194/os-10-1047-2014.

Buermann W, Dong J, Zeng X, Myneni RB, Dickinson RE. 2001. Evaluation of the utility of satellite-based vegetation leaf area index data for climate simulations. *J Clim* **14**(17): 3536–3550. doi: 10.1175/1520-0442(2001)014<3536:eotuos>2.0.co;2.

Chen HS, Wang ZF, Li J, Tang X, Ge BZ, et al. 2015. GNAQPMS-Hg v1.0, a global nested atmospheric mercury transport model: Model description, evaluation and application to trans-boundary transport of Chinese anthropogenic emissions. *Geosci Model Dev* **8**(9): 2857–2876. doi: 10.5194/gmd-8-2857-2015.

Cheng I, Zhang L, Mao H, Blanchard P, Tordon R, et al. 2014. Seasonal and diurnal patterns of speciated atmospheric mercury at a coastal-rural and a coastal-urban site. *Atmos Environ* **82**(0): 193–205. doi: 10.1016/j.atmosenv.2013.10.016.

Choi H-D, Holsen TM. 2009. Gaseous mercury fluxes from the forest floor of the Adirondacks. *Environ Pollut* **157**(2): 592–600. doi: 10.1016/j.envpol.2008.08.020.

Ci ZJ, Zhang XS, Wang ZW. 2011a. Elemental mercury in coastal seawater of Yellow Sea, China: Temporal variation and air–sea exchange. *Atmos Environ* **45**(1): 183–190. doi: 10.1016/j.atmosenv.2010.09.025.

Ci ZJ, Zhang XS, Wang ZW, Niu ZC, Diao XY, et al. 2011b. Distribution and air-sea exchange of mercury (Hg) in the Yellow Sea. *Atmos Chem Phys* **11**(6): 2881–2892. doi: 10.5194/acp-11-2881-2011.

Converse AD, Riscassi AL, Scanlon TM. 2010. Seasonal variability in gaseous mercury fluxes measured in a high-elevation meadow. *Atmos Environ* **44**(18): 2176–2185. doi: 10.1016/j.atmosenv.2010.03.024.

Corbitt ES, Jacob DJ, Holmes CD, Streets DG, Sunderland EM. 2011. Global source–receptor relationships for mercury deposition under present-day and 2050 emissions scenarios. *Environ Sci Technol* **45**(24): 10477–10484. doi: 10.1021/es202496y.

Cui L, Feng X, Lin C-J, Wang X, Meng B, et al. 2014. Accumulation and translocation of ^{198}Hg in four crop species. *Environ Toxicol Chem* **33**(2): 334–340. doi: 10.1002/etc.2443.

Dastoor A, Ryzhkov A, Durnford D, Lehnherr I, Steffen A, et al. 2015. Atmospheric mercury in the Canadian Arctic. Part II: Insight from modeling. *Sci Total Environ* **509–510**: 16–27. doi: 10.1016/j.scitotenv.2014.10.112.

De Simone F, Gencarelli CN, Hedgecock IM, Pirrone N. 2014. Global atmospheric cycle of mercury: A model study on the impact of oxidation mechanisms. *Environ Sci Pollut R* **21**(6): 4110–4123. doi: 10.1007/s11356-013-2451-x.

Driscoll CT, Mason RP, Chan HM, Jacob DJ, Pirrone N. 2013. Mercury as a global pollutant: Sources, pathways, and effects. *Environ Sci Technol* **47**(10): 4967–4983. doi: 10.1021/es305071v.

Drummond MA, Loveland TR. 2010. Land-use pressure and a transition to forest-cover loss in the eastern United States. *BioScience* **60**(4): 286–298. doi: 10.1525/bio.2010.60.4.7.

Ebinghaus R, Jennings SG, Schroeder WH, Berg T, Donaghy T, et al. 1999. International field intercomparison measurements of atmospheric mercury species at Mace Head, Ireland. *Atmos Environ* **33**(18): 3063–3073. doi: 10.1016/S1352-2310(98)00119-8.

Environment Canada. 2013. The 2011 National Pollutant Release Inventory downloadable datasets [dataset]. http://www.ec.gc.ca/inrp-npri/. Accessed February 2, 2016.

Fay L, Gustin M. 2007. Assessing the influence of different atmospheric and soil mercury concentrations on foliar mercury concentrations in a controlled environment. *Water Air Soil Pollut* **181**(1–4): 373–384. doi: 10.1007/s11270-006-9308-6.

Ferrari CP, Gauchard P-A, Aspmo K, Dommergue A, Magand O, et al. 2005. Snow-to-air exchanges of mercury in an Arctic seasonal snow pack in Ny-Ålesund, Svalbard. *Atmos Environ* **39**(39): 7633–7645. doi: 10.1016/j.atmosenv.2005.06.058.

Fritsche J, Obrist D, Zeeman MJ, Conen F, Eugster W, et al. 2008. Elemental mercury fluxes over a sub-alpine grassland determined with two micrometeorological methods. *Atmos Environ* **42**(13): 2922–2933. doi: 10.1016/j.atmosenv.2007.12.055.

Fu X, Feng X, Zhu W, Rothenberg S, Yao H, et al. 2010. Elevated atmospheric deposition and dynamics of mercury in a remote upland forest of southwestern China. *Environ Pollut* **158**(6): 2324–2333. doi: 10.1016/j.envpol.2010.01.032.

Gårdfeldt K, Sommar J, Ferrara R, Ceccarini C, Lanzillotta E, et al. 2003. Evasion of mercury from coastal and open waters of the Atlantic Ocean and the Mediterranean Sea. *Atmos Environ* **37**(Supplement 1): 73–84. doi: 10.1016/S1352-2310(03)00238-3.

Gay DA, Schmeltz D, Prestbo E, Olson M, Sharac T, et al. 2013. The Atmospheric Mercury Network: Measurement and initial examination of an ongoing atmospheric mercury record across North America. *Atmos Chem Phys* **13**(22): 11339–11349. doi: 10.5194/acp-13-11339-2013.

Goodsite ME, Plane JMC, Skov H. 2004. A theoretical study of the oxidation of Hg^0 to $HgBr_2$ in the troposphere. *Environ Sci Technol* **38**(6): 1772–1776. doi: 10.1021/Es034680s.

Goodsite ME, Plane JMC, Skov H. 2012. Correction to a theoretical study of the oxidation of Hg^0 to $HgBr_2$ in the troposphere. *Environ Sci Technol* **46**(9): 5262–5262. doi: 10.1021/es301201c.

Gratz LE, Ambrose JL, Jaffe DA, Knote C, Jaeglé L, et al. Airborne observations of mercury emissions from the Chicago/Gary urban/industrial area during the 2013 NOMADSS campaign. *Elem Sci Anth*: in preparation.

Gratz LE, Ambrose JL, Jaffe DA, Shah V, Jaeglé L, et al. 2015. Oxidation of mercury by bromine in the subtropical Pacific free troposphere. *Geophys Res Lett* **42**(23): 10494–10502. doi: 10.1002/2015GL066645.

Gustin MS, Engle M, Ericksen J, Lyman S, Stamenkovic J, et al. 2006. Mercury exchange between the atmosphere and low mercury containing substrates. *Appl Geochem* **21**(11): 1913–1923. doi: 10.1016/j.apgeochem.2006.08.007.

Gustin MS, Lindberg SE. 2005. Terrestial Hg fluxes: Is the net exchange up, down, or neither?, in Pirrone N, Mahaffey KR, eds., *Dynamics of Mercury Pollution on Regional and Global Scales*. New York, NY, USA: Springer.

Holmes CD, Jacob DJ, Corbitt ES, Mao J, Yang X, et al. 2010. Global atmospheric model for mercury including oxidation by bromine atoms. *Atmos Chem Phys* **10**(24): 12037–12057. doi: 10.5194/acp-10-12037-2010.

Holtslag AAM, Boville BA. 1993. Local versus nonlocal boundary-layer diffusion in a global climate model. *J Clim* **6**(10): 1825–1842. doi: 10.1175/1520-0442(1993)006<1825:LVNBLD>2.0.CO;2.

Jung G, Hedgecock IM, Pirrone N. 2009. ECHMERIT V1.0 – a new global fully coupled mercury-chemistry and transport model. *Geosci Model Dev* **2**(2): 175–195. doi: 10.5194/gmd-2-175-2009.

Kikuchi T, Ikemoto H, Takahashi K, Hasome H, Ueda H. 2013. Parameterizing soil emission and atmospheric oxidation-reduction in a model of the global biogeochemical cycle of mercury. *Environ Sci Technol* **47**(21): 12266–12274. doi:10.1021/es401105h.

Kim PS, Jacob DJ, Fisher JA, Travis K, Yu K, et al. 2015. Sources, seasonality, and trends of southeast US aerosol: An integrated analysis of surface, aircraft, and satellite observations with the GEOS-Chem chemical transport model. *Atmos Chem Phys* **15**(18): 10411–10433. doi: 10.5194/acp-15-10411-2015.

Kuss J, Zülicke C, Pohl C, Schneider B. 2011. Atlantic mercury emission determined from continuous analysis of the elemental mercury sea-air concentration difference within transects between 50°N and 50°S. *Global Biogeochem Cy* **25**(3): GB3021. doi: 10.1029/2010gb003998.

Lei H, Liang XZ, Wuebbles DJ, Tao Z. 2013. Model analyses of atmospheric mercury: Present air quality and effects of transpacific transport on the United States. *Atmos Chem Phys* **13**(21): 10807–10825. doi: 10.5194/acp-13-10807-2013.

Li W, Li L, Fu R, Deng Y, Wang H. 2011. Changes to the North Atlantic Subtropical High and its role in the intensification of summer rainfall variability in the Southeastern United States. *J Clim* **24**(5): 1499–1506. doi: 10.1175/2010jcli3829.1.

Li W, Li L, Ting M, Liu Y. 2012. Intensification of Northern Hemisphere subtropical highs in a warming climate. *Nature Geosci* **5**(11): 830–834. doi: 10.1038/ngeo1590.

Lin C-J, Gustin MS, Singhasuk P, Eckley C, Miller M. 2010. Empirical models for estimating mercury flux from soils. *Environ Sci Technol* **44**(22): 8522–8528. doi: 10.1021/es1021735.

Lin C-J, Pehkonen SO. 1999. The chemistry of atmospheric mercury: A review. *Atmos Environ* **33**(13): 2067–2079. doi: 10.1016/s1352-2310(98)00387-2.

Lin J-T, McElroy MB. 2010. Impacts of boundary layer mixing on pollutant vertical profiles in the lower troposphere: Implications to satellite remote sensing. *Atmos Environ* **44**(14): 1726–1739. doi: 10.1016/j.atmosenv.2010.02.009.

Lindberg S, Bullock R, Ebinghaus R, Engstrom D, Feng X, et al. 2007. A synthesis of progress and uncertainties in attributing the sources of mercury in deposition. *AMBIO* **36**(1): 19–33. doi: 10.1579/0044-7447(2007)36[19:asopau]2.0.co;2.

Lindberg SE, Turner RR. 1977. Mercury emissions from chlorine-production solid waste deposits. *Nature* **268**(5616): 133–136.

Liss PS, Slater PG. 1974. Flux of gases across the air-sea interface. *Nature* **247**: 181–184. doi: 10.1038/247181a0.

Liu S, Liang X-Z. 2010. Observed diurnal cycle climatology of planetary boundary layer height. *J Clim* **23**(21): 5790–5809. doi: 10.1175/2010jcli3552.1.

Lyman SN, Jaffe DA. 2012. Formation and fate of oxidized mercury in the upper troposphere and lower stratosphere. *Nature Geosci* **5**(2): 114–117. doi: 10.1038/ngeo1353.

Maestas MM. 2011. Characterization of speciated atmospheric mercury concentration measurements in northern Utah [Thesis]. Salt Lake City, Utah, USA: University of Utah, Department of Atmospheric Sciences. http://content.lib.utah.edu/cdm/ref/collection/etd3/id/202. Accessed February 2, 2016.

Mao H, Talbot RW, Sigler JM, Sive BC, Hegarty JD. 2008. Seasonal and diurnal variations of Hg^0 over New England. *Atmos Chem Phys* **8**(5): 1403–1421. doi: 10.5194/acp-8-1403-2008.

Mason RP. 2009. Mercury emissions from natural processes and their importance in the global mercury cycle, in Mason RP, Pirrone N, eds., *Mercury Fate and Transport in the Global Atmosphere*. New York, NY, USA: Springer.

Mason RP, Sheu GR. 2002. Role of the ocean in the global mercury cycle. *Global Biogeochem Cy* **16**(4): 1093. doi: 10.1029/2001gb001440.

Miller SM, Wofsy SC, Michalak AM, Kort EA, Andrews AE, et al. 2013. Anthropogenic emissions of methane in the United States. *P Natl Acad Sci USA*. **110**(50): 20018–20022. doi: 10.1073/pnas.1314392110.

Nightingale PD, Malin G, Law CS, Watson AJ, Liss PS, et al. 2000. In situ evaluation of air-sea gas exchange parameterizations using novel conservative and volatile tracers. *Global Biogeochem Cy* **14**(1): 373–387. doi: 10.1029/1999gb900091.

Obrist D, Gustin MS, Arnone III JA, Johnson DW, Schorran DE, et al. 2005. Measurements of gaseous elemental mercury fluxes over intact tallgrass prairie monoliths during one full year. *Atmos Environ* **39**(5): 957–965. doi: 10.1016/j.atmosenv.2004.09.081.

Obrist D, Pokharel AK, Moore C. 2014. Vertical profile measurements of soil air suggest immobilization of gaseous elemental mercury in mineral soil. *Environ Sci Technol* **48**(4): 2242–2252. doi: 10.1021/es4048297.

Pacyna EG, Pacyna JM, Sundseth K, Munthe J, Kindbom K, et al. 2010. Global emission of mercury to the atmosphere from anthropogenic sources in 2005 and projections to 2020. *Atmos Environ* **44**(20): 2487–2499. doi: 10.1016/j.atmosenv.2009.06.009.

Parrella JP, Jacob DJ, Liang Q, Zhang Y, Mickley LJ, et al. 2012. Tropospheric bromine chemistry: Implications for present and pre-industrial ozone and mercury. *Atmos Chem Phys* **12**(15): 6723–6740. doi: 10.5194/acp-12-6723-2012.

Pirrone N, Cinnirella S, Feng XB, Finkelman RB, Friedli HR, et al. 2010. Global mercury emissions to the atmosphere from anthropogenic and natural sources. *Atmos Chem Phys* **10**(13): 5951–5964. doi: 10.5194/acp-10-5951-2010.

Poissant L, Pilote M, Constant P, Beauvais C, Zhang HH, et al. 2004. Mercury gas exchanges over selected bare soil and flooded sites in the bay St. François wetlands (Québec, Canada). *Atmos Environ* **38**(25): 4205–4214. doi: 10.1016/j.atmosenv.2004.03.068.

Pongprueksa P, Lin CJ, Singhasuk P, Pan L, Ho TC, et al. 2011. Application of CMAQ at a hemispheric scale for atmospheric mercury simulations. *Geosci Model Dev Discuss* **4**(3): 1723–1754. doi: 10.5194/gmdd-4-1723-2011.

Prestbo EM, Gay DA. 2009. Wet deposition of mercury in the U.S. and Canada, 1996–2005: Results and analysis of the NADP mercury deposition network (MDN). *Atmos Environ* **43**(27): 4223–4233. doi: 10.1016/j.atmosenv.2009.05.028.

Rosner B, Grove D. 1999. Use of the Mann–Whitney *U*-test for clustered data. *Stat Med* **18**(11): 1387–1400. doi: 10.1002/(SICI)1097-0258(19990615)18:11<1387::AID-SIM126>3.0.CO;2-V.

Ridley BA, Grahek FE. 1990. A small, low flow, high sensitivity reaction vessel for NO chemiluminescence detectors. *J Atmos Oceanic Technol* **7**(2): 307–311. doi: 10.1175/1520-0426(1990)007<0307:aslfhs>2.0.co;2.

Schmidt JA, Jacob DJ, Horowitz HM, Hu L, Sherwen T, et al. 2015. Modeling the observed tropospheric BrO background: Importance of multiphase chemistry and implications for ozone, OH, and mercury. *J Geophys Res*: submitted.

Seidel DJ, Ao CO, Li K. 2010. Estimating climatological planetary boundary layer heights from radiosonde observations: Comparison of methods and uncertainty analysis. *J Geophys Res-Atmos* **115**(D16). doi: 10.1029/2009jd013680.

Seinfeld JH, Pandis SN. 2006. *Atmospheric Chemistry and Physics: From Air Pollution to Climate Change*. 2nd ed. Hoboken, New Jersey, USA: Wiley-Interscience.

Selin NE. 2009. Global biogeochemical cycling of mercury: A review. *Annu Rev Env Resour* **34**(1): 43–63. doi: 10.1146/annurev.environ.051308.084314.

Selin NE, Jacob DJ, Park RJ, Yantosca RM, Strode S, et al. 2007. Chemical cycling and deposition of atmospheric mercury: Global constraints from observations. *J Geophys Res-Atmos* **112**(D2). doi: 10.1029/2006jd007450.

Selin NE, Jacob DJ, Yantosca RM, Strode S, Jaeglé L, et al. 2008. Global 3-D land-ocean-atmosphere model for mercury: Present-day versus preindustrial cycles and anthropogenic enrichment factors for deposition. *Global Biogeochem Cy* **22**(2): GB2011. doi: 10.1029/2007gb003040.

Shah V, Jaeglé L, Gratz LE, Ambrose JL, Jaffe DA, et al. 2016. Origin of oxidized mercury in the summertime free troposphere over the southeastern US. *Atmos Chem Phys* **16**(3): 1511–1530. doi: 10.5194/acp-16-1511-2016.

Shetty SK, Lin C-J, Streets DG, Jang C. 2008. Model estimate of mercury emission from natural sources in East Asia. *Atmos Environ* **42**(37): 8674–8685. doi: 10.1016/j.atmosenv.2008.08.026.

Slemr F, Angot H, Dommergue A, Magand O, Barret M, et al. 2015. Comparison of mercury concentrations measured at several sites in the Southern Hemisphere. *Atmos Chem Phys* **15**(6): 3125–3133. doi: 10.5194/acp-15-3125-2015.

Slemr F, Weigelt A, Ebinghaus R, Brenninkmeijer C, Baker A, et al. 2014. Mercury plumes in the global upper troposphere observed during flights with the CARIBIC observatory from May 2005 until June 2013. *Atmosphere* **5**(2): 342. doi: 10.3390/atmos5020342.

Smith-Downey NV, Sunderland EM, Jacob DJ. 2010. Anthropogenic impacts on global storage and emissions of mercury from terrestrial soils: Insights from a new global model. *J Geophys Res-Biogeo* **115**(G3): G03008. doi: 10.1029/2009jg001124.

Soerensen AL, Mason RP, Balcom PH, Jacob DJ, Zhang Y, et al. 2014. Elemental mercury concentrations and fluxes in the tropical atmosphere and ocean. *Environ Sci Technol* **48**(19): 11312–11319. doi: 10.1021/es503109p.

Soerensen AL, Mason RP, Balcom PH, Sunderland EM. 2013. Drivers of surface ocean mercury concentrations and air–sea exchange in the West Atlantic Ocean. *Environ Sci Technol* **47**(14): 7757–7765. doi: 10.1021/es401354q.

Soerensen AL, Sunderland EM, Holmes CD, Jacob DJ, Yantosca RM, et al. 2010. An improved global model for air-sea exchange of mercury: High concentrations over the North Atlantic. *Environ Sci Technol* **44**(22): 8574–8580. doi: 10.1021/es102032g.

Song S, Selin NE, Soerensen AL, Angot H, Artz R, et al. 2015. Top-down constraints on atmospheric mercury emissions and implications for global biogeochemical cycling. *Atmos Chem Phys* **15**(12): 7103–7125. doi: 10.5194/acp-15-7103-2015.

Sprovieri F, Pirrone N, Ebinghaus R, Kock H, Dommergue A. 2010. A review of worldwide atmospheric mercury measurements. *Atmos Chem Phys* **10**(17): 8245–8265. doi: 10.5194/acp-10-8245-2010.

Stamenkovic J, Gustin MS. 2009. Nonstomatal versus stomatal uptake of atmospheric mercury. *Environ Sci Technol* **43**(5): 1367–1372. doi: 10.1021/es801583a.

Strode SA, Jaeglé L, Selin NE, Jacob DJ, Park RJ, et al. 2007. Air-sea exchange in the global mercury cycle. *Global Biogeochem Cy* **21**(1): GB1017. doi: 10.1029/2006gb002766.

Sunderland EM, Dalziel J, Heyes A, Branfireun BA, Krabbenhoft DP, et al. 2010. Response of a macrotidal estuary to changes in anthropogenic mercury loading between 1850 and 2000. *Environ Sci Technol* **44**(5): 1698–1704. doi: 10.1021/es9032524.

Sunderland EM, Mason RP. 2007. Human impacts on open ocean mercury concentrations. *Global Biogeochem Cy* **21**(4): GB4022. doi: 10.1029/2006gb002876.

Temme C, Ebinghaus R, Kock HH, Schwerin A, Bieber E. 2006. Field intercomparison of mercury measurements within EMEP (executive summary). http://www.nilu.no/projects/ccc/qa/files/EMEP-QA_Hg_UBA.doc. Accessed February 2, 2016.

U.S. EPA. 2013. The 2011 National Emissions Inventory [dataset]. http://www.epa.gov/ttnchie1/net/2011inventory.html. Accessed February 2, 2016.

U.S. EPA. 2015. The Toxics Release Inventory (TRI) Program. http://www2.epa.gov/toxics-release-inventory-tri-program. Accessed February 2, 2016.

van der Werf GR, Randerson JT, Giglio L, Collatz GJ, Mu M, et al. 2010. Global fire emissions and the contribution of deforestation, savanna, forest, agricultural, and peat fires (1997–2009). *Atmos Chem Phys* **10**(23): 11707–11735. doi: 10.5194/acp-10-11707-2010.

Wang D, He L, Shi X, Wei S, Feng X. 2006. Release flux of mercury from different environmental surfaces in Chongqing, China. *Chemosphere* **64**(11): 1845–1854. doi: 10.1016/j.chemosphere.2006.01.054.

Wang S, Schmidt JA, Baidar S, Coburn S, Dix B, et al. 2015. Active and widespread halogen chemistry in the tropical and subtropical free troposphere. *P Natl Acad Sci USA*. **112**(30): 9281–9286. doi: 10.1073/pnas.1505142112.

Wang X, Lin CJ, Feng X. 2014. Sensitivity analysis of an updated bidirectional air–surface exchange model for elemental mercury vapor. *Atmos Chem Phys* **14**(12): 6273–6287. doi: 10.5194/acp-14-6273-2014.

Weigelt A, Ebinghaus R, Manning AJ, Derwent RG, Simmonds PG, et al. 2015. Analysis and interpretation of 18 years of mercury observations since 1996 at Mace Head, Ireland. *Atmos Environ* **100**: 85–93. doi: 10.1016/j.atmosenv.2014.10.050.

Wesely ML. 1989. Parameterization of surface resistances to gaseous dry deposition in regional-scale numerical models. *Atmos Environ* **23**(6): 1293–1304. doi: 10.1016/0004-6981(89)90153-4.

Xiao ZF, Munthe J, Schroeder WH, Lindqvist O. 1991. Vertical fluxes of volatile mercury over forest soil and lake surfaces in Sweden. *Tellus B* **43**(3): 267–279. doi: 10.1034/j.1600-0889.1990.t01-1-00009.x-i1.

Xu X, Yang X, Miller DR, Helble JJ, Carley RJ. 1999. Formulation of bi-directional atmosphere-surface exchanges of elemental mercury. *Atmos Environ* **33**(27): 4345–4355. doi: 10.1016/S1352-2310(99)00245-9.

Yuan B, Kaser L, Karl T, Graus M, Peischl J, et al. 2015. Airborne flux measurements of methane and volatile organic compounds over the Haynesville and Marcellus shale gas production regions. *J Geophys Res-Atmos* **120**(12): 6271–6289. doi: 10.1002/2015jd023242.

Zhang LM, Wright LP, Blanchard P. 2009. A review of current knowledge concerning dry deposition of atmospheric mercury. *Atmos Environ* **43**(37): 5853–5864. doi: 10.1016/j.atmosenv.2009.08.019.

Zhang Y, Jaeglé L, Thompson L, Streets DG. 2014. Six centuries of changing oceanic mercury. *Global Biogeochem Cy* **28**(11): 1251–1261. doi: 10.1002/2014gb004939.

Zhang Y, Jaeglé L, van Donkelaar A, Martin RV, Holmes CD, et al. 2012. Nested-grid simulation of mercury over North America. *Atmos Chem Phys* **12**(14): 6095–6111. doi: 10.5194/acp-12-6095-2012.

Contributions

- Conception and design: SS, NES, DAJ, LJ
- Acquisition of observational data: LEG, JLA, DAJ, BY, LK, ECA, RSH, NJB, AJW, RLM III, CAC, MSC, GC, TMH, WTL, RT
- Analysis and interpretation of data: SS, NES, LEG, JLA
- Drafted and/or revised the article: SS, NES, LEG, DAJ, VS, LJ, AG, BY, LK, NJB, AJW, CAC, TMH
- Approved the submitted version for publication: SS, NES, DAJ

Acknowledgments

We thank the NCAR's Earth Observing Laboratory and its Research Aviation Facility for their support throughout NOMADSS. We acknowledge Wisconsin Department of Natural Resources, Oklahoma Cherokee Nation Air Quality Program, and all the other site operators and principal investigators within the NADP AMNet for providing observational data used in this study. We also thank two reviewers for constructive comments.

Funding information

The U.S. NSF provides funding for the NOMADSS project (#1217010 to DAJ, LJ, and NES and #1216743 to CAC and RLM III). SS and NES acknowledge the U.S. NSF Atmospheric Chemistry Program #1053648. SS also thanks the MIT Henry Houghton Fund for travel support.

Competing interests

The authors have declared that no competing interests exist.

Supplemental material

- **Figure S1. Vertical profile of potential temperature observed during all the NOMADSS research flights.**
  The altitude of 0–4 km is shown. Each black circle is an individual 2.5 minute observational data point merged based on the sampling interval of the DOHGS. The red line displays the medians of potential temperature for each 0.2 km vertical bin. The dashed blue line indicates the altitude of 1.2 km which is one of the two criteria to select observations within the PBL. This altitude is determined by inspecting the vertical profile of potential temperature. Within 1.2 km, potential temperature is nearly constant with height; whereas above 1.2 km, it increases sharply with altitude. (EPS) doi: 10.12952/journal.elementa.000100.s001
- **Figure S2. The wet deposition data measured by the NADP MDN and its comparison with different model simulations in 2013 summer.**
  The plot in (**a**) shows the spatial distribution of measurement sites in the eastern North America. The plot in (**b**) shows the model–observation comparison for REF, INV, and HOXSO. The gray solid lines indicate 1:2, 1:1, and 2:1 ratios, respectively. (EPS) doi: 10.12952/journal.elementa.000100.s002

- **Figure S3. Examples of temporal changes in river water discharge from South Carolina into the Northwest Atlantic during recent years and measurements of precipitation rate and wet deposition flux of mercury in South Carolina during 2013 summer.**
  The plot in (**a**) shows daily water discharges of the Edisto River measured at a USGS station (No. 02175000) near Givhans, South Carolina, from 2011–2014. Notice that vertical axis is expressed in a log scale, and that the highest water discharge during recent years was measured in July 2013. The plot in (**b**) shows measurements at a NADP Mercury Deposition Network (MDN) station (No. SC05; 32.9430° N, 79.6592° W) in 2013 summer. Both precipitation rate and Hg wet deposition peaked from June 19 to July 2, 2013, right before the over-water sampling dates (July 5 and 8, 2013) of the two NOMADSS research flights (RF-14 and RF-16). Similar temporal patterns of river water discharges, precipitation rates, and Hg wet deposition fluxes can be found for other stations in South Carolina on the USGS web page (http://waterdata.usgs.gov/usa/nwis/) and on the NADP MDN web page (http://nadp.sws.uiuc.edu/mdn/). (EPS) doi: 10.12952/journal.elementa.000100.s003
- **Figure S4. Seasonal variability and spatial distribution of modeled net oceanic Hg^0 flux from the North Atlantic.**
  Results of the model simulation HOXSO are shown. The modeled net oceanic Hg^0 fluxes for different seasons are plotted in (a) December–January–February, (b) March–April–May, (c) June–July–August, and (d) September–October–November. (EPS) doi: 10.12952/journal.elementa.000100.s004
- **Table S1. A summary of measured net emission fluxes of Hg^0 for different land uses and seasons. (PDF)** doi: 10.12952/journal.elementa.000100.s005

Data accessibility statement

The NOMADSS observational data are publicly available from the SAS project on the NCAR/UCAR Earth Observing Laboratory's website (http://data.eol.ucar.edu/master_list/?project=SAS). The NADP AMNet observational data are available on the NADP's website (http://nadp.sws.uiuc.edu/data/AMNet/) but access to these data is password protected (please contact the program coordinator). Ship cruise data are published in Soerensen et al. (2013). GEOS-Chem is an open source chemical transport model for atmospheric composition (http://www.geos-chem.org). Model simulation results are available upon request.